Numerical investigation into cavitating flow around a NACA66 hydrofoil with DCM models

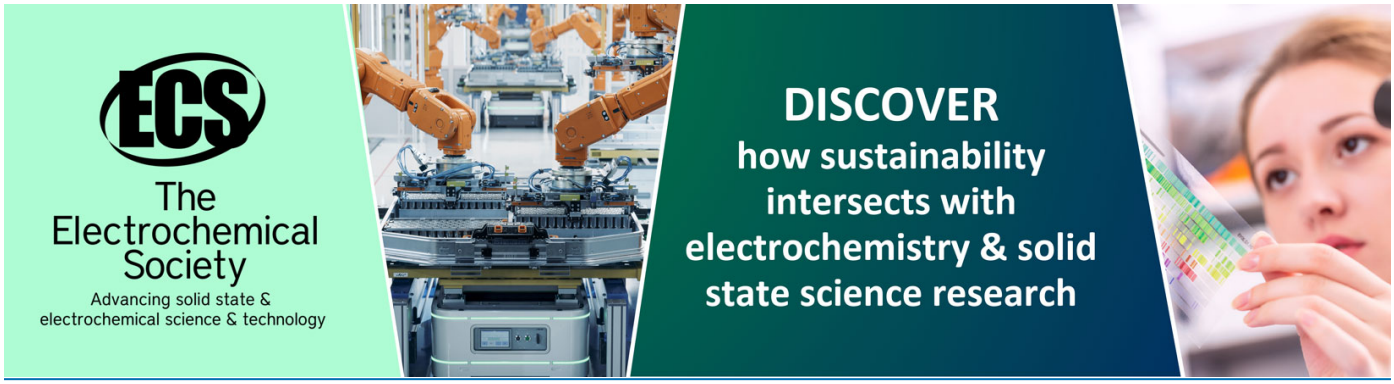

Numerical investigation into cavitating flow around a NACA66 hydrofoil with DCM models

L G Sun, P C Guo, X B Zheng, J G Yan, J J Feng and X Q Luo

State Key Laboratory of Eco-hydraulics in Northwest Arid Region, Xi'an University of Technology, Xi'an 710048, Shaanxi Province, China

E-mail: sunlg_xut@126.com

Abstract. Unsteady cavitating flow is difficult to be predicted accurately with traditional RANS turbulence model, especially cavities shedding and evolution from sheet cavity to cloud cavity. In order to determine an appropriate numerical setup for accurate and reliable simulations of cavitating flow, the unsteady-state cavitating flow simulations are performed with the Zwart cavitation model accompanying with the DCM(Density correction model) model based on the RNG k-ε turbulence model after grid convergence test. The details about pressure distribution and cavities evolution around the hydrofoil show that the used models predict the cavities shedding frequency well, the pressure distribution along chord is quasi-periodic. Due to the dynamic of the shed cavities, periodic lift and drag coefficient are pretty clear with both positive and negative values. The cavities formation, breakup, shedding and collapse in a cycle are also presented.

1. Introduction

Cavitating flow in hydraulic machines has continuously attracted the attentions of researchers in recent years, resulting from its negative consequences on operation stability, such as undesirable cavitation erosion, reduction in efficiency, vibration and noise. Credible estimation of cavitation characteristic is vital during design stage, due to the lives of blades are significantly deteriorated by cavitation. For example, the traveling bubble development in the storage pump, inlet edge cavitation and cavitation whirl in Francis turbine, as well as tip clearance and hub cavitation for Kaplan runner[1, 2].

The cavitating flow around hydrofoil or runner/impeller tends to be treated numerically in the early stage, since its strengths of saving investment and increasing predictive accuracy. The accuracy of cavitation modeling depends both on turbulence model and cavitation model. Most cavitation model is based on the Rayleigh-Plesset equation or its simplified formula, which assumes that the liquid carries cavitation nuclei whose growth is controlled by the Rayleigh-Plesset equation[3]. Furthermore, the

turbulence model plays a vital role to capture cavitation[4]. Ji B[5] et al. reproduced the attached cavity and the shedding U-shaped horse-shoe vortex around a twisted hydrofoil by using the Partially-Averaged Navier–Stokes (PANS) method and a mass transfer cavitation model. Peters A[6] et al. simulated the cavitation erosion over a NACA 0009 hydrofoil with an Euler multiphase flow solver in combination with an erosion model on the basis of microjet hypothesis, the prediction of cavitation erosion was compared to experimental tests. A numerical investigation of cavitating flow on a NACA 0015 hydrofoil was performed by Capurso T [7] et al. to predict to the interaction between sheet and cloud cavitation by means of open source code OpenFOAM, in term of RANS approach and two types of transitional turbulence model.

In addition, cavitation-vortex interaction was employed by Ji B[8] and Zhao Y[9] respectively, to shed light on the influence of cavitation on the vorticity distribution and the contribution of different terms stemming from the vorticity transport equation to cavitation development. Furthermore, the Lagrangian-based method was used to investigate the unsteady cavitating flow. The determined ridge can form a Lagrangian coherent structures to represent the movement trajectory of the fluid particle[10]. Long X[11] et al. developed a three dimensional Lagrangian technology to straightforwardly display the track lines of re-entrant and side-entrant jets, evolution of U- type structures and the interactions between cavitation and vortices. A multiscale two-phase model based on a coupled Eulerian/Lagrangian approach was developed by Hsiao C-T[12] et al. to model and capture the sheet and cloud cavitation dynamics. The proposed multiscale model consists in a micro-scale model, a macro-scale model, a transition scheme and yields to a very good validation of the modeling of 2D NACA0015 hydrofoil.

The presented paper is intended to contribute to the understanding of how cavitation formation, breakup, shedding and collapse with special emphasis on evolution from sheet cavities to cloud cavities. The unsteady-state cavitating flow simulations are performed with the Zwart cavitation model accompanying with the DCM(Density correction model) model based on the RNG k-ε turbulence model. The time-resolved pressure, cavity development are also discussed.

2. Numerical model in cavitation calculation

2.1. Continuity and momentum equations

The governing equations hypothesize the cavitating flow of mixture of water and vapor keep uniformity, where the multiphase fluid components are assumed to share the same velocity and pressure. The continuity and momentum equations for the mixture flow in the Cartesian coordinates are as follows:

$$\frac{\partial \rho_m}{\partial t}+\frac{\partial\left(\rho_m u_j\right)}{\partial x_j}=0 \tag{1}$$

$$\frac{\partial\left(\rho_m u_i\right)}{\partial t}+\frac{\partial\left(\rho_m u_i u_j\right)}{\partial x_j}=-\frac{\partial \rho}{\partial x_i}+\frac{\partial}{\partial x_j}\left[\left(\mu_m+\mu_t\right)\left(\frac{\partial u_i}{\partial x_j}+\frac{\partial u_j}{\partial x_i}-\frac{2}{3}\frac{\partial u_k}{\partial x_k}\delta_{ij}\right)\right] \tag{2}$$

$$\rho_m=\rho_v\alpha_v+\rho_l\alpha_l \tag{3}$$

$$\mu_m = \mu_v \alpha_v + \mu_l \alpha_l \tag{4}$$

where ρ_m is the mixture density, μ_m and μ_t are the mixture laminar viscosity and turbulent viscosity respecitively, u is the velocity, α is the volume fraction, δ is Kronecker delta function. The subscripts (*i, j, k*) denote the components related to the appropriate cartesian coordinates and (*v, l*) correspond to liquid and vapor phase respectively.

2.2. Cavitation model and Density correction model

According to the Zwart cavitation model derived from a simplified Rayleigh–Plesset equation and integrated inside ANSYS-CFX, the vapor volume fraction is governed by the following equation:

$$\frac{\partial(\rho_v \alpha_v)}{\partial t} + \frac{\partial(\rho_v \alpha_v u_j)}{\partial x_j} = \dot{m}^+ - \dot{m}^- \tag{5}$$

The source term $\dot{m}^+$ and the sink term $\dot{m}^-$ in Eq.(5) refer to the condensation and evaporation rates respectively, which are defined as follows:

$$\dot{m}^+ = C_{evap} \frac{3\alpha_{nuc}\alpha_l \rho_v}{R_b} \sqrt{\frac{2}{3}\frac{Max(p_v - p, 0)}{\rho_l}} \tag{6}$$

$$\dot{m}^- = C_{cond} \frac{3\alpha_v \rho_v}{R_b} \sqrt{\frac{2}{3}\frac{Max(p - p_v, 0)}{\rho_l}} \tag{7}$$

where C_{evap} and C_{cond} are empirical coefficients for the vaporization and the condensation, α_{nuc} denotes the nucleation volume fraction, R_b denotes the bubble diameter, p and p_v are the local fluid pressure and the saturated liquid vapor pressure respectively. By default, $C_{evap} = 40$, $C_{cond} = 0.01$, $\alpha_{nuc} = 5 \times 10^{-4}$ and $R_b = 1 \times 10^{-6}$.

The RNG k-ε model is developed for incompressible single phase flow and over-predicts the turbulence kinetic energy as well as the turbulent viscosity. Coutier[13] et al. developed a local compressibility correction for turbulent viscosity to improve the simulation accuracy of cavitation flowing, where the turbulent viscosity is corrected by function of $f(\rho)$.

$$\mu_t = f(\rho)\frac{C_\mu k^2}{\varepsilon} \tag{8}$$

$$f(\rho) = \rho_v + \left(\frac{\rho_v - \rho}{\rho_v - \rho_l}\right)^n (\rho_l - \rho_v) \tag{9}$$

where $C_\mu = 0.09$ and $n = 10$.

3. Calculation model and grid generation

3.1. Geometry parameters and boundary conditions

In this research, the NACA66 hydrofoil with nominal angle of incidence of 6° was numerically investigated to perform cavitation characteristic according to Leroux J-B[14]. Figure 1. shows the cross section of 3D hydrofoil geometry with cavitation tunnel of 1.2m long and 0.192m wide. The chord length was c=0.15m and the span length was 0.192m. The hydrofoil was located in 2c upstream of the leading edge and 6c downstream of the leading edge. During cavitation simulation, the cavitation number is $\sigma = 1.25$ and saturated liquid vapor pressure at 25℃ is $P_v = 2970Pa$.

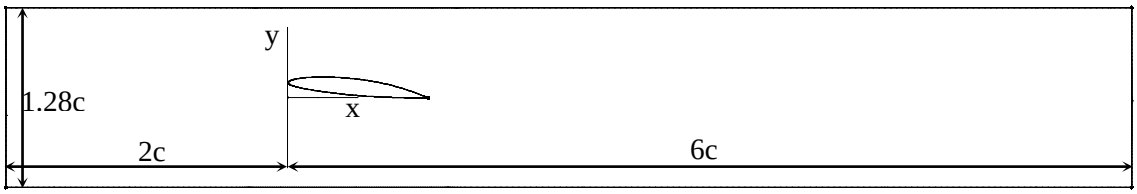

Figure 1. Main dimensions of fluid domain.

The velocity inlet boundary conditions $U_\infty = 5.33m/s$ was prescribed and the outlet was treated as a static gauge pressure outlet in terms of the cavitation number $\sigma = (P_2 - P_v)/(0.5\rho_l U_\infty)$. The high resolution was used for advection scheme and turbulence numerics, with second order backward Euler used for transient scheme. All the cavitating flow simulations had been run with a time step size $\Delta t = c/(200U_\infty) = 1.4071\times10^{-4}s$, a maximum of 60 iterations for one inner loop was required to achieve the set accuracy (Max residual $\leq 10^{-3}$) using the selected time step size. A no-slip boundary condition is imposed on the hydrofoil surface, and free-slip are imposed on the top and bottom walls of the tunnel. All cavitating runs have been initialized with fully wetted calculations results under steady state.

3.2. Grid generation and grid convergence test

The computational domain has been discretized by means of an O-H type grid with sufficient refinement near the hydrofoil surface. In order to perform a grid-convergence test, the widely accepted grid convergence index (GCI) based on Richardson extrapolation method was used to estimate the discretization errors described by Celik I and Trivedi C[15, 16]. The GCI is an indicator with a 95% confidence interval of how far the finer of the two compared grids is to the asymptotic value and predicts how further refinement affects the solution. The discretization error with three different densities shown in figure 2.(fine, G1; medium, G2; and coarse, G3) is determined as follows:
Step *1*. Define a representative average grid size *h*.

$$h = \left[\frac{1}{N}\sum_{i=1}^{N}(\Delta V_i)\right]^{1/3} \tag{10}$$

where ΔV_i is a cell volume and *N* is the total number of elements used for the simulations.

Step *2*. Let $h_1 < h_2 < h_3$, the grid refinement factor is $r_{21} = h_2/h_1$ and $r_{32} = h_3/h_2$ respectively, and it is suggested that *r* is greater than 1.3.

Step *3*. Calculate the apparent order p with fixed-point iteration.

$$p = \frac{1}{\ln(r_{21})}\left|\ln\left|\varepsilon_{32}/\varepsilon_{21}\right| + \ln(\frac{r_{21}^{p}-s}{r_{32}^{p}-s})\right| \tag{11}$$

where $s = 1\cdot\mathrm{sgn}(\varepsilon_{32}/\varepsilon_{21})$, $\varepsilon_{21} = \phi_2 - \phi_1$, $\varepsilon_{32} = \phi_2 - \phi_1$, and ϕ is a critical variable being investigated.

Step *4*. Calculate extrapolated values.

$$\phi_{ext}^{21} = \frac{\left(r_{21}^{p}\phi_1 - \phi_2\right)}{r_{21}^{p}-1} \tag{12}$$

Step *5*. The approximate relative error e_a, extrapolated relative error e_{ext} and grid convergence index *GCI* can be determined.

$$e_a^{21} = \left|\frac{\phi_2-\phi_1}{\phi_1}\right|,\quad e_{ext}^{21} = \left|\frac{\phi_{ext}^{21}-\phi_1}{\phi_{ext}^{21}}\right|,\quad GCI_{21} = \frac{1.25e_a^{21}}{r_{21}^{p}-1} \tag{13}$$

similarly, calculate e_a^{32}, e_{ext}^{32}, GCI_{32}.

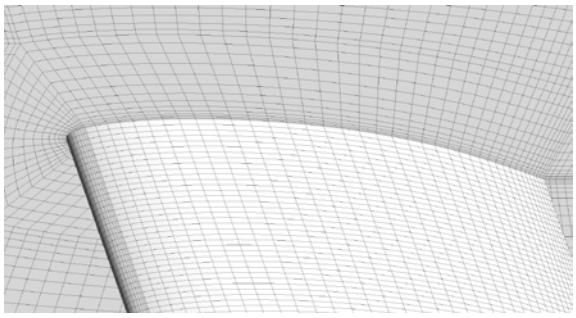

(a) G3

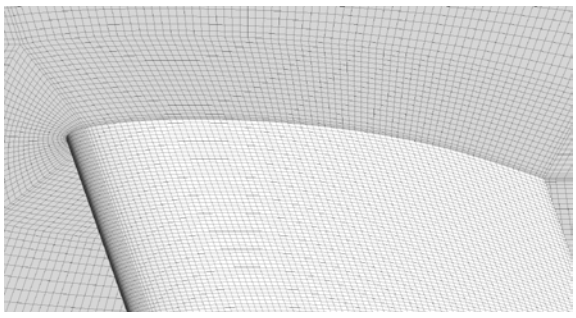

(a) G2

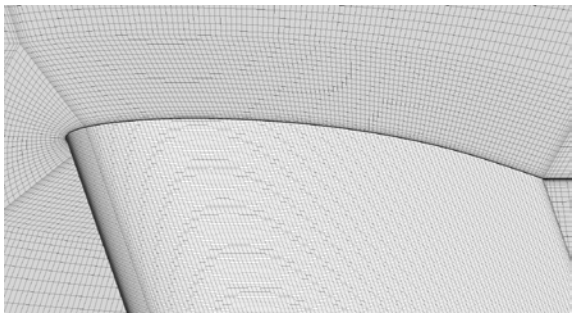

(a) G1

Figure 2. The grid views with three densities.

The calculation procedure for three selected grids are tabulated in table 1.

Taking into account the lift and drag coefficient as the critical variable as shown in table 1. It is observed that all grid converge in a monotonic manner, which are indicative of the average flow field certainly benefits from grid refinement. The numerical uncertainty in CL around the foil was calculated to be 3.87% and 2.31% for the medium and fine grid densities respectively, and CD error was 3.47% and 1.54%. In order to provide an adequate balance between computational expense and accuracy, the medium grid was chosen as the best compromise.

Table 1. Statistics for discretization error and uncertainties in numerical solutions.

Parameter	Lift coefficient(CL)			Drag coefficient(CD)		
N_1, N_2, N_3	9329529,	4240695,	1570627	9329529,	4240695,	1570627
h_1, h_2, h_3	1.6726e-3,	2.1752e-3,	3.0289e-3	1.6726e-3,	2.1752e-3,	3.0289e-3
ϕ_1, ϕ_2, ϕ_3	1.6923,	1.6718,	1.6259	0.1729,	0.1703,	0.1621
r_{21}, r_{32}	1.3006,	1.3925		1.3006,	1.3925	
$\varepsilon_{21}, \varepsilon_{32}$	-0.0205,	-0.0459		-0.0026,	-0.0082	
p	1.9160			3.0386		
$\phi_{ext}^{21}, \phi_{ext}^{32}$	1.7236,	1.7236		0.1750,	0.1750	
e_a^{21}, e_a^{32}	0.0121,	0.0275		0.0150,	0.0482	
$e_{ext}^{21}, e_{ext}^{32}$	0.0301,	0.0567		0.0270,	0.0739	
GCI_{21}, GCI_{32}	0.0231,	0.0387		0.0154,	0.0347	

4. Numerical results and discussion

4.1. Pressure Distribution

Figure 3. shows the time-dependent pressure and FFT analysis at chord of 0.8c consisted with Ref.[14]. The pressure distribution is quasi-periodic except for some discrepancy in peak pressure. The predicted cavitation shedding frequency is about 3.5533Hz, which is in good agreement with the experimental result of 3.625Hz. The numerical observations are indicative of the modified turbulent eddy viscosity enables to capture the shedding of the vapor cloud.

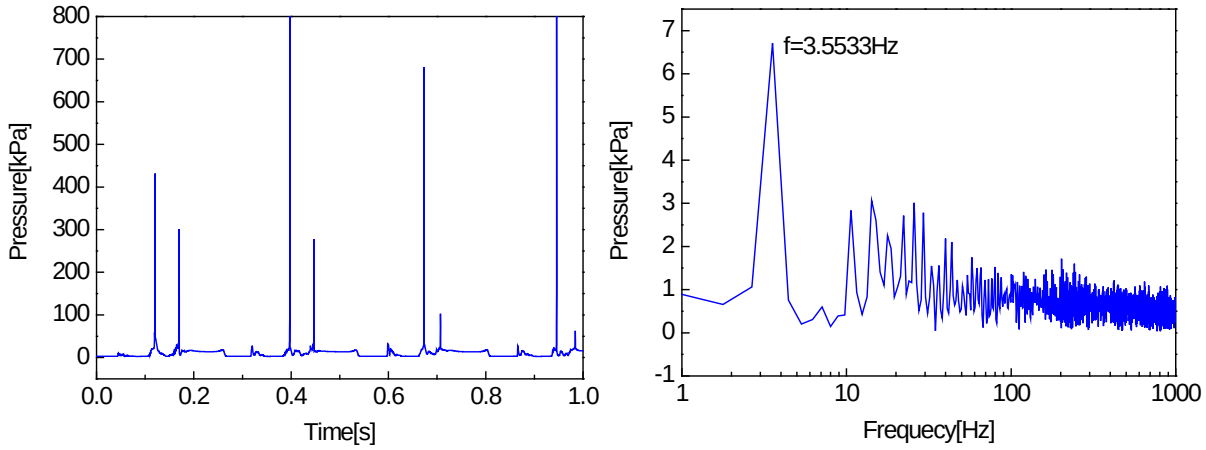

(a) Temporal variation of pressure (b) FFT analysis

Figure 3. Time-dependent pressure and FFT analysis at chord of 0.8c.

Figure 4. reports the lift and drag coefficient signal as a function of time. It shows the cyclic time signal and the periods are pretty clear with both positive and negative values. The phenomenon is mainly attributed to the dynamic of the shed cavities which are driven by the main flow-field downstream of the cavity closure. It should be noted that every cycle is very different and irreproducible due to cavitation and cavities shedding instability. At the moment of cavity collapse and shedding, the lift coefficient decreases to below minus 1.

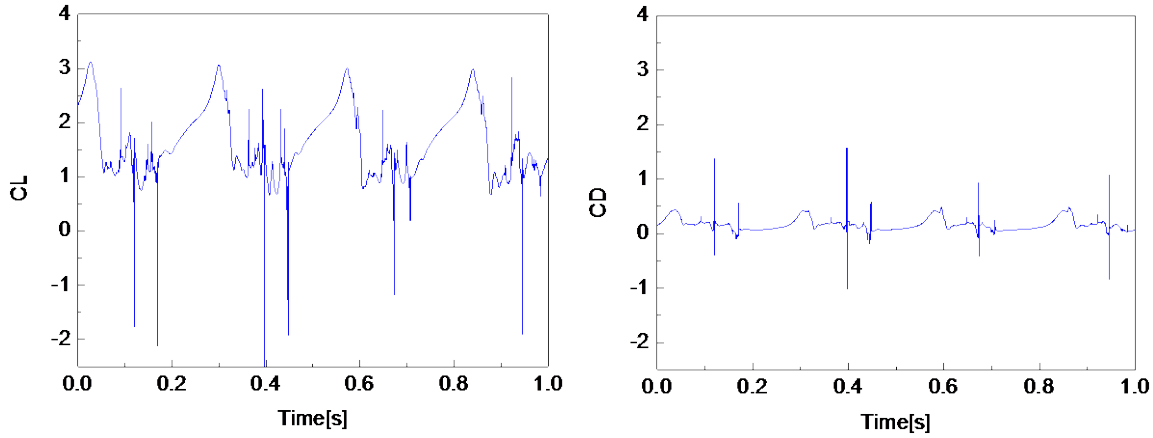

(a) Lift coefficient (b) Drag coeficient

Figure 4. Time evolutions of lift and drag coefficient signal.

4.2. Cavitation evolution from sheet cavities to cloud cavities

The cavitation evolution obtained from simulations, are compared with those of experimental in a cycle is depicted in figure 5. The experimental observations and numerical solution are respectively illustrated on the left and right side. The comparisons between the details experimental data and CFD

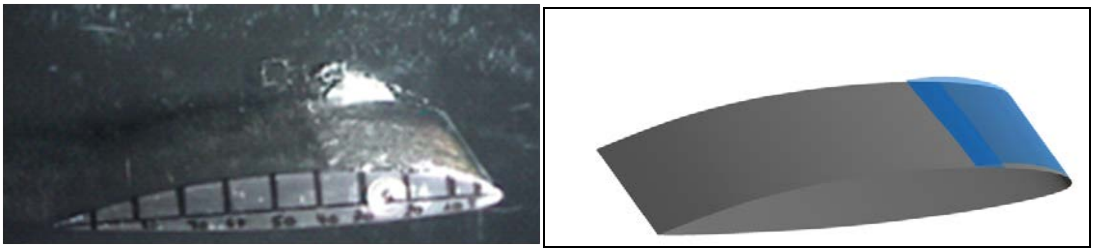

(a) 1/8T

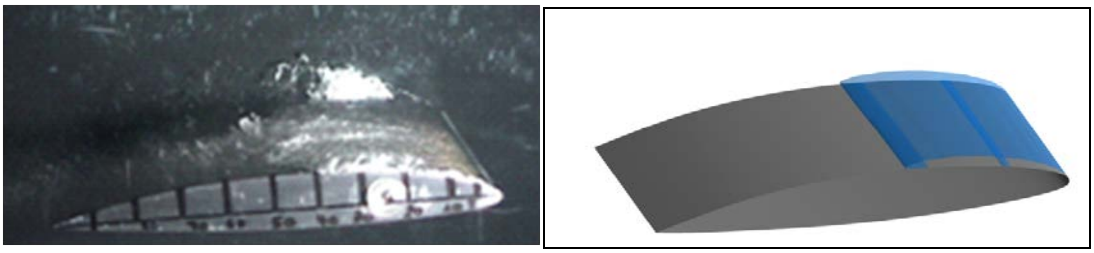

(b) 2/8T

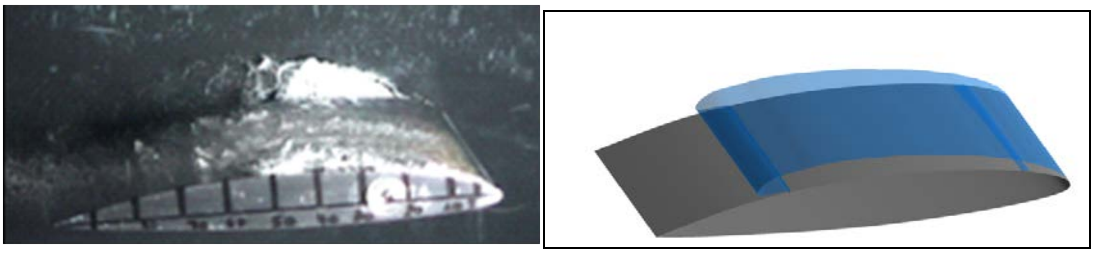

(c) 3/8T

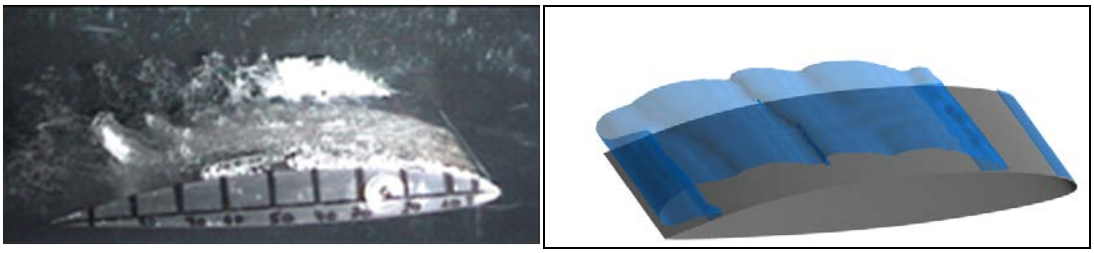

(d) 4/8T

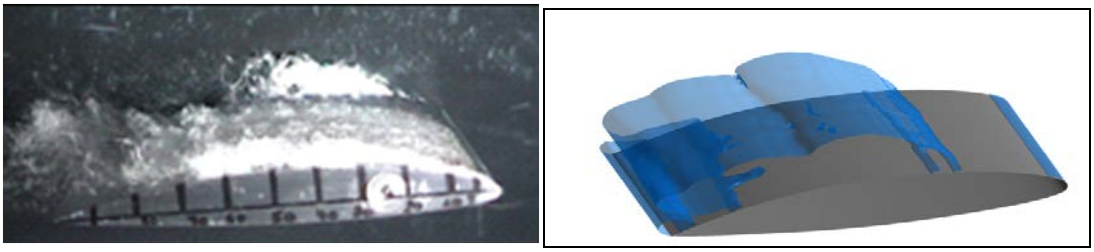

(e) 5/8T

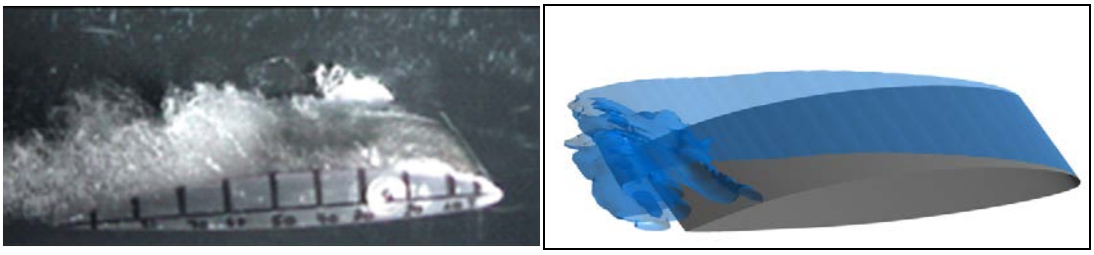

(f) 6/8T

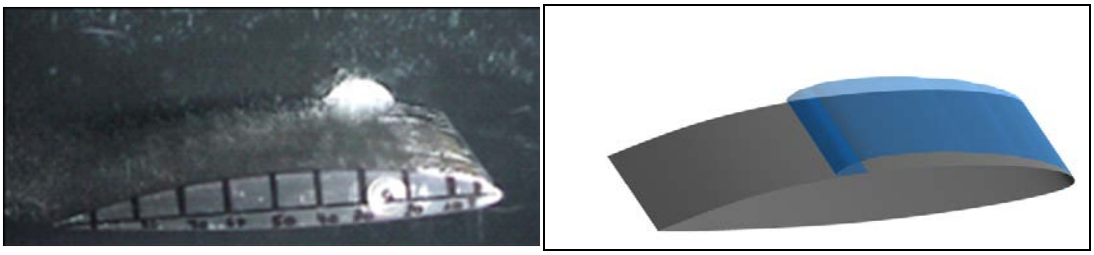

(g) 7/8T

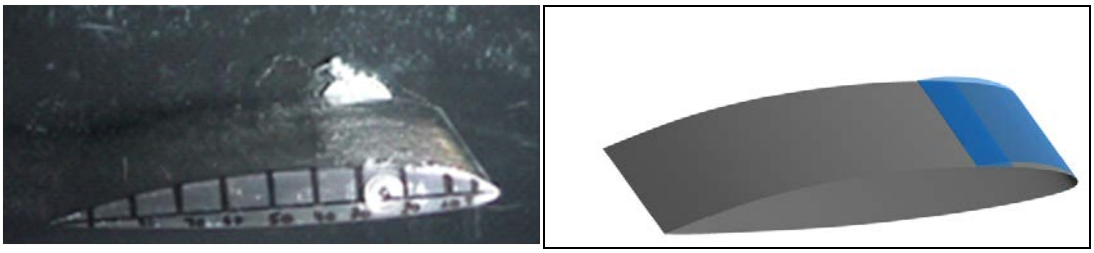

(h) 8/8T

Figure 5. Instantaneous snap-shots of unsteady cavitation evolution.

simulations yields to a good validation of the modeling of time evolution of the cavity from steady sheet and unsteady cloud cavity.

The numerical model has capability to predict the cavity initiation, growth towards the trailing edge and subsequent shedding. At time of 1/8T, sheet cavity starts to develop and attaches to the foil at the leading edge. Soon afterwards, the attached cavity length increases with slight reentrant jet flow. By

the time of 3/8T, the sheet cavity is always maintained, indicating the cavitating flow is stabilized. After 4/8T, cavity break up occurs at the leading edge and the cavity develops from sheet to unsteady cloud cavity at trailing edge reported in figure 5. (d) and (e), at this time the reentrant jet flow is fully developed and its maximum values. Cavity reattachment to foil at leading edge is observed and reaches coexistence of sheet and cloud cavity at time of 6/8T. Subsequently, the unsteady cloud cavity collapses rapidly and leaves only sheet cavity before a new begins again, see figure 5. (g) and (h).

5. Conclusion

A transient numerical investigation into cavitating flow around a NACA66 hydrofoil with DCM models was performed in this paper. The grid convergence test is conducted by the method of GCI and the pressure distribution and cavity evolution from sheet to cloud cavity is discussed.

The pressure distribution along foil chord is quasi-periodic and predicted cavity shedding frequency is well validated against the experimental attain. Due to the dynamic of the shed cavities, periodic lift and drag coefficient are pretty clear with both positive and negative values, however, it is irreproducible. The cavities experience sheet cavity formation and growth, breakup, cloud cavity development, shedding and collapse in a cycle.

Acknowledgement

This work was supported by the National Natural Science Foundation of China(Grant No. 51479166, 51339005), the Key Research and Development Program of Shaanxi Province(Grant No. 2017ZDXM-GY-081) and the Scientific Research Program of Shaanxi Provincial Education Department (Grant No. 17JF019).

References

[1] Avellan F 2004 Introduction to cavitation in hydraulic machinery. In: *6th International Conference on Hydraulic Machinery and Hydrodynamics,* (Timisoara, Romania pp 11-22

[2] Luo X-w, Ji B and Tsujimoto Y 2016 A review of cavitation in hydraulic machinery *Journal of Hydrodynamics, Ser. B* **28** 335-58

[3] Franc J-P 2007 *Fluid Dynamics of Cavitation and Cavitating Turbopumps,* ed L d'Agostino and M V Salvetti (Vienna: Springer Vienna) pp 1-41

[4] Huang B, Young Y L, Wang G and Shyy W 2013 Combined Experimental and Computational Investigation of Unsteady Structure of Sheet/Cloud Cavitation *Journal of Fluids Engineering* **135** 071301--16

[5] Ji B, Luo X, Wu Y, Peng X and Duan Y 2013 Numerical analysis of unsteady cavitating turbulent flow and shedding horse-shoe vortex structure around a twisted hydrofoil *International Journal of Multiphase Flow* **51** 33-43

[6] Peters A, Sagar H, Lantermann U and el Moctar O 2015 Numerical modelling and prediction of cavitation erosion *Wear* **338-339** 189-201

[7] Capurso T, Lopez M, Lorusso M, Torresi M, Pascazio G, Camporeale S M and Fortunato B 2017 Numerical investigation of cavitation on a NACA0015 hydrofoil by means of OpenFOAM *Energy Procedia* **126** 794-801

[8] Ji B, Luo X, Arndt R E A and Wu Y 2014 Numerical simulation of three dimensional cavitation shedding dynamics with special emphasis on cavitation–vortex interaction *Ocean Engineering* **87** 64-77
[9] Zhao Y, Wang G and Huang B 2016 Vortex structure analysis of unsteady cloud cavitating flows around a hydrofoil *Modern Physics Letters B* **30** 1550275
[10] Haller G and Yuan G 2000 Lagrangian coherent structures and mixing in two-dimensional turbulence *Physica D: Nonlinear Phenomena* **147** 352-70
[11] Long X, Cheng H, Ji B, Arndt R E A and Peng X 2018 Large eddy simulation and Euler–Lagrangian coupling investigation of the transient cavitating turbulent flow around a twisted hydrofoil *International Journal of Multiphase Flow* **100** 41-56
[12] Hsiao C-T, Ma J and Chahine G L 2017 Multiscale tow-phase flow modeling of sheet and cloud cavitation *International Journal of Multiphase Flow* **90** 102-17
[13] Coutier-Delgosha O, Fortes-Patella R and Reboud J L 2003 Evaluation of the Turbulence Model Influence on the Numerical Simulations of Unsteady Cavitation *Journal of Fluids Engineering* **125** 38-45
[14] Leroux J-B, Astolfi J A and Billard J Y 2004 An Experimental Study of Unsteady Partial Cavitation *Journal of Fluids Engineering* **126** 94-101
[15] Celik I, Ghia U, Roache P J, Freitas C, Coloman H and Raad P 2008 Procedure for Estimation and Reporting of Uncertainty Due to Discretization in CFD Applications *Journal of Fluids Engineering* **130** 078001--4
[16] Trivedi C 2017 Investigations of Compressible Turbulent Flow in a High-Head Francis Turbine *Journal of Fluids Engineering* **140** 011101--17